The International Journal of Advanced Manufacturing Technology (2020) 109:335–344
https://doi.org/10.1007/s00170-020-05578-2

ORIGINAL ARTICLE

# Study on the influence of pre-stress time-characteristic on microstructure transformation in GH process

Yijing Niu[1] · Yunlong Yao[1] · Shichao Xiu[1]

Received: 4 March 2020 / Accepted: 2 June 2020 / Published online: 1 July 2020


**Abstract**
Firstly, simulation is used to analyze the temperature curve in pre-stress hardening grinding (PSHG). Then, according to the start and the end time of martensitic transformation, three time nodes are selected to study the pre-stress time characteristic; they are 1 s, 3 s, and 7 s after grinding. The influence of pre-stress on the initial temperature and content of martensite transformation in cooling is analyzed; the results indicate the content of martensite increases over the pre-stressed unloading time. To test the theory, experiments of PSHG with different unloading times are carried out. The microstructure of the grinding hardening surface is observed and explored by scanning electron microscopy (SEM). Then, the SEM images are binarized to get the martensite content on the hardening surface. The experimental results show martensite content is consistent with the theoretical analysis. Lath martensite and flake martensite can also be found in these pictures. Flake martensite slightly increases while unloading at 7 s, as it forms at a lower temperature. So the pre-stress time characteristic influences both the martensite content and the morphology of martensite formed.

**Keywords** Pre-stress time characteristic · Pre-stress hardening grinding · Martensitic transformation · Fake martensite

## 1 Introduction

The increasing miniaturization of electronic and mechanical devices requires certain surfaces to be finished to a high degree of hardness, roughness, residual stress, etc. Further progress of their development is expected not only in the wide application of new structural materials but also in improving the properties of traditional materials by controlling their chemical composition and structural state [1–4].

In 1996, Brinksmeier et al. proposed to use the enormous amount of heat generated in the contact zone to produce the strengthened layer of parts [5]. The new technique was named grind hardening (GH). They found that GH was a surface self-quenching process, where martensite transformation took place by short-time austenitization. After that, the hardness, strength, and impact resistance of the workpiece were all improved, which will benefit the working performance such as wear resistance, corrosion resistance, and so on [6, 7].

However, the tensile residual stress is easily got in the hardening layer due to the effect of grinding heat and force [8]. Residual compressive stress improves the service life, while residual tensile stress has an opposite effect [9]. Surface residual tensile stress is often found in the heat-treated component, which is harmful to the working performance of the workpiece [10].

If a certain thickness of the strengthened layer and residual compressive stress can be obtained after GH, it will greatly improve the properties of the workpiece. Controlling residual stress is difficult for machining technology studying. The shot peening and vibration aging process are routine means for controlling residual stress [11, 12]. Although these methods can control residual stress, they cannot be used in GH.

In 2015, Xiu et al. proposed a pre-stress combined with GH to gain residual compressive stress on a machined surface [13]. It uses the inner metal elastic deformation recovery to reduce the tensile residual stresses [14]. Shi et al. studied the PSHG from different pre-stress, grinding depth, and feeding speed of a workpiece and found these parameters had an obvious influence on the grinding hardening layer [15].

✉ Shichao Xiu
358716263@qq.com

Yijing Niu
21710320@qq.com

Yunlong Yao
1396717435@qq.com

[1] School of Mechanical Engineering and Automation, Northeastern University, Heping Region Wenhua Road, Shenyang 110819, China

To further study the effect of the pre-stress on microstructure transformation during grinding, the pre-stress time characteristic study is proposed. Three time nodes are selected to study the pre-stress time characteristic. Pre-stress raises the starting temperature of martensite formation (Ms), and it can also increase the fraction of martensite formed. To test the theory, the experiment is carried out. Experimental results prove that pre-stress changes the morphology and properties of martensite formed.

## 2 Grinding temperature simulation

### 2.1 Heat source model for GH

The moving heat source theory has been widely used by most analyses that have been developed to predict the temperature rise at the grinding zone [16–18]. The heat source is arranged on the circular arc of the contact surface between the wheel and the workpiece, and it is the sum of infinite moving line sources [19]. Therefore, the circular arc of the heat source model is established in this study, as in Fig. 1.

The contact arc is equally divided into $n$ parts; the value of moving heat source in different parts can be written as:

$$q_i = i^2 \times \left(3q_{\mathrm{w}}/\mathrm{n}^2\right) \tag{1}$$

The heat transferred into the workpiece causes the temperature of the workpiece surface to rise. The total heat flux $q$ in the grinding region is calculated from the tangential grinding force.

$$q = \frac{F_{\mathrm{t}}(v_{\mathrm{s}} - v_{\mathrm{w}})}{bl_{\mathrm{g}}} \tag{2}$$

where $v_{\mathrm{s}}$ is the wheel speed, $v_{\mathrm{w}}$ is the feed rate of the wheel, $b$ is the width, $F_{\mathrm{t}}$ is the tangential grinding force, and $l_{\mathrm{g}}$ is the contact arc length.

$$F_{\mathrm{t}} = 28282 \times \left(a_{\mathrm{p}}\right)^{0.86}(v_{\mathrm{s}})^{-1.06}(v_{\mathrm{w}})^{0.44} \tag{3}$$

$$l_{\mathrm{g}} = \sqrt{a_{\mathrm{p}} d_{\mathrm{s}}} \tag{4}$$

where $a_{\mathrm{p}}$ is grinding depth, and $d_{\mathrm{s}}$ is the wheel diameter.

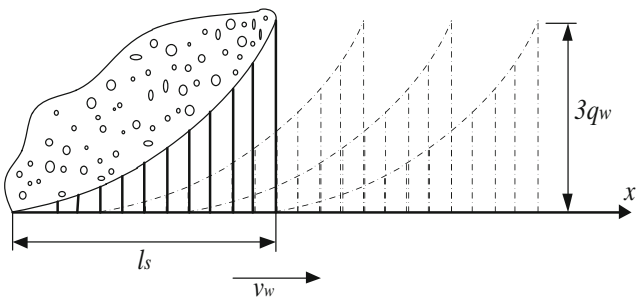


**Fig. 1** Moving heat source model

The moving heat source transferred into the workpiece can be calculated by the heat distribution ratio:

$$q_{\mathrm{w}} = \varepsilon q \tag{5}$$

The heat distribution coefficient $\varepsilon$ is derived from the contact model of the grinding zone [20, 21]:

$$\varepsilon = \frac{1}{1 + \sqrt{\dfrac{(k\rho c)_{\mathrm{s}}}{(k\rho c)_{\mathrm{w}}}}} \tag{6}$$

where $(k\rho c)_{\mathrm{w}}$ and $(k\rho c)_{\mathrm{s}}$ are the thermal characteristics of the workpiece and the grinding wheel.

### 2.2 Simulation parameters (Table 1)

### 2.3 Calculation of temperature field

In grinding, the workpiece material undergoes complex phase transformation. Therefore, latent heat produced by phase transformation is an important reason affecting the temperature field. The change in phase transformation latent heat with time and temperature is nonlinear. Phase transformation latent heat in this simulation is achieved by considering the specific heat capacity at different temperatures.

Then considering the heat conduction and initial and boundary conditions, the temperature field is simulated.

### 2.4 Grinding temperature

The transient temperature field can be obtained by cyclically loading heat source. And the temperature field distribution can be obtained in Fig. 2.

Figure 3 shows the temperature curve at a point on the surface of the workpiece. The highest temperature is set to be 0 s, and the temperature exceeds 1000 °C. The temperature falls quickly then slowly after grinding. To study the pre-stress time characteristic on martensitic transformation, the pre-

**Table 1** Simulation parameters

| Grinding simulation | Parameters |
|---|---|
| Grinding mode | Dry grinding, up-grinding |
| Wheel speed $v_{\mathrm{s}}$ | 30 m/s |
| Feed rate $v_{\mathrm{w}}$ | 200mm/min |
| Grinding depth $a_{\mathrm{p}}$ | 0.15 mm |
| Grinding width $b$ | 10 mm |
| Wheel diameter $d_{\mathrm{s}}$ | 350 mm |
| Workpiece material | AISI1045 |
| Heat distribution coefficient | 0.4 [22] |
| Room temperature | 20 °C |

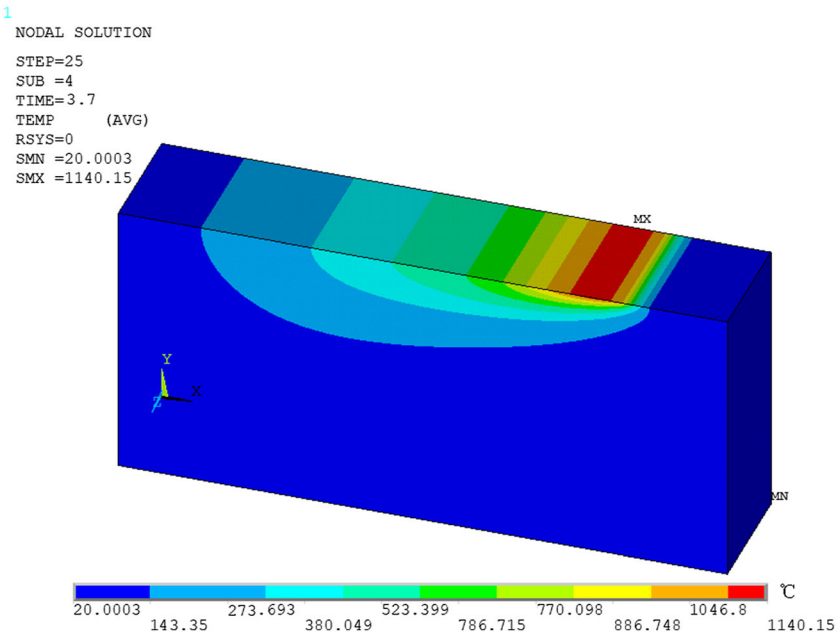


**Fig. 2** The distributions of temperature field

stress unloads during cooling. Here, three time nodes are selected to study the pre-stress time-characteristic. They are before $M_s(t_u = 1s)$, during martensitic transformation ($t_u = 3s$), and after the martensitic transformation is done due to temperature that decreased slowly ($t_u = 7s$).

## 3 The effect of pre-stress on martensitic transformation

### 3.1 The transformation process

The formation of grinding hardening surface is a complex process of structural transformation under the combined action of grinding force and grinding heat. In this process, external stress plays a positive role in the transformation of structure.

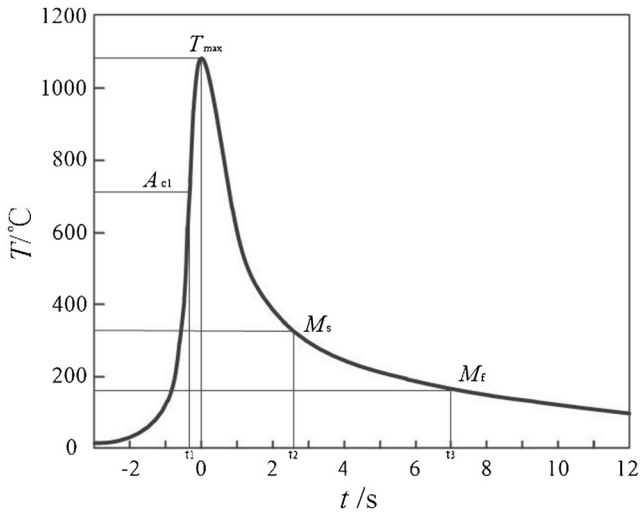


**Fig. 3** Temperature curve

When the temperature exceeds $A_{c1}(t_1)$, ferrite and pearlite transform to austenite at the same time. With the increase in temperature, the austenization becomes increasingly obvious. Meanwhile, grain coarsening accompanies the whole heating due to the grains' competitive growth.

As the grinding wheel passes by, the temperature reaches the highest point, and then it starts to fall. When the time arrives $t_2$, the temperature drops down to $M_s$. The martensitic transformation starts after the temperature is just below $M_s$.

Pre-stress changes the starting temperature of martensite formation and the morphology and properties of martensite formed [23, 24].

### 3.2 The effect of pre-stress on $M_s$

The free energy change $\Delta G^{\gamma \to M}$ associated with the martensitic transformation in Fe-C can be expressed as [25, 26]

$$\Delta G^{\gamma \to M} = \Delta G^{\gamma \to \alpha} + \Delta G^{\alpha \to M} \tag{7}$$

where $\Delta G^{\gamma \to \alpha}$ is the free energy change accompanying face-centered cubic (fcc) ($\gamma$)→body-centered cubic (bcc), or body-centered tetragonal (bct) ($\alpha$), and it is also the driving force of the martensite transformation.

$$\Delta G^{\gamma \to \alpha} = \Delta G_{Fe}^{\gamma \to \alpha} + 4.184 \times (10500 - 3.425T) \tag{8}$$

$\Delta G_{Fe}^{\gamma \to \alpha}$ is the free energy change accompanying fcc($\gamma$)→bcc or bct($\alpha$) for pure iron, and it can be written as

$$\Delta G_{Fe}^{\gamma \to \alpha} = -1661.59 - 530.8 \times 10^{-2} T - 16.92 \times 10^{-4} \times T^2 + 124.5 \times 10^{-2} T \ln T \tag{9}$$

$\Delta G^{\alpha \to M}$ is the free energy change forming martensite from fcc, and it is also called transformation resistance.

$$\Delta G^{\alpha \to M} = 2.1\sigma_{M_s}^{0.2} + 900 \tag{10}$$

where $\sigma_{M_s}^{0.2}$ is the yield strength of austenite at $M_s$.

$$\sigma_{M_s}^{0.2} = 130 + 2800x_c + 0.2 \times (800 - T) \tag{11}$$

$M_s$ can be calculated as $\Delta G^{\gamma \to M} = 0$.

When the external stress $\sigma$ is applied at $T_1 (T_1 > M_s)$, the mechanical driving force $\Delta G_{mech}$ due to the external stress $\sigma$ is added to the chemical driving force $\Delta G_{T_1}$. When the total driving force $\Delta G_{T_1} + \Delta G_{mech}$ is equal to the critical stress $\Delta G_{M_S}^{\gamma \to M}$, the stress-induced martensitic transformation starts [27].

$$\Delta G_{M_s}^{\gamma \to M} = \Delta G_{T_1} + \Delta G_{mech} \tag{12}$$

For an external uniaxial tensile or compressive stress $\sigma$, the associated mechanical driving force $\Delta G_{mech}$ can be expressed as

$$\Delta G_{mech} = \frac{1}{2}\sigma[\gamma \sin 2\theta \cos\alpha \pm \varepsilon(1 + \cos 2\theta)] \tag{13}$$

where "-" represents compressive stress, and "+" represents tensile stress; the latter is adopted in this paper. $\gamma$ is the shear strain along the transformation shear direction on a habit plane. $\varepsilon$ is the normal component of the transformation strain. $\theta$ is the angle between the axis of applied stress and the normal to the habit plane. $\alpha$ is the angle between the shear direction of the transformation and the maximum shear direction of the applied stress on the habit plane.

A martensite plate, whose orientation yields a maximum value of mechanical driving force $\Delta G_{mech}$, will be formed. The maximum value $\Delta G_{mech}$ is obtained when $\alpha = 0$ and $d\Delta G_{mech}/d\theta = 0$. $\theta = 41^\circ$ can be obtained, using $\gamma = 0.22$ and $\varepsilon = 0.03$ as values for the martensitic transformation [28].

$$\Delta G_{mech} = 0.126\sigma \mathrm{Jmol}^{-1} \tag{14}$$

As the degree of supercooling required to reach the appropriate driving force for initiating the reaction is reduced, and the $M_s$ temperature is thereby raised to $M_s'$ by the applied stress.

Patel and Cohen gave an equation expressing the effect of external stress on the $M_s'$ as [29]

$$\frac{dM_s'}{d\sigma} = \frac{\Delta G_{mech}}{d(\Delta G^{\gamma\alpha})/dT} = \frac{0.126\sigma}{6.79} \mathrm{KMPa}^{-1} \tag{15}$$

where $\Delta G^{\gamma\alpha}$ is the driving force. Equation (15) suggests applied pre-stress for the start of the martensite transformation in the present steel is expected to increase linearly with an increase in pre-stress.

### 3.3 Amount of martensite under different pre-stress unloading times

For martensitic transformation, the following formula is used [30, 31].

$$f = 1 - \exp\left[-\alpha\left(M_s' - T\right)\right] \tag{16}$$

where $\alpha$ depends on the material of the steel, and it is also affected by external stress [26].

$$\alpha = 1.243 \times 10^{-2} - 6.9752 \times 10^{-5}\sigma \tag{17}$$

The martensitic transformation can be divided into two parts based on the cooling as in Fig. 4. In section A, for the grinding temperature $T_{max} < T < M_s(M_s')$, the fraction of martensite stays at zero. In section B, for the temperature $M_s(M_s') < T < M_f$, the fraction of martensite increases as the temperature drops down. While for the temperature $T < M_f$, the cooling rate becomes slow, and austenite becomes thermally stabilized due to a slow temperature drop. Therefore, the transformation of martensite is retarded. The growth of martensite almost stops after $M_f$ [32].

As seen in Fig. 4, the content curve of martensite rises with the decrease of temperature under different pre-stress unloading times. When unloading pre-stress at $t_u = 1s$, the external stress does not affect the martensitic transformation. The onset temperature of the martensitic transformation is still $M_s$. At the same time, the external stress does not work on the growth of martensite due to unloading. Besides, pre-stress does not affect martensitic transformation when unloading external stress from 0 to $t_2(M_s)$. So the growth of martensite will be the same as unloading pre-stress between 0 and $t_2$, and the content curve is the same as unloading at 1 s.

The quantity of martensite depends on temperature. Therefore, when the temperature drops just below $M_s(M_s')$, a small part of the martensite forms quickly. As the temperature keeps falling, another part of martensite forms. As a result, the transformation continues in a stress-free state after unloading the external stress.

When unloading pre-stress at $t_u = 3s$, the temperature is about 300 °C. The onset of martensitic transformation raises to $M_s'$ due to external stress, so the transformation takes place earlier. Meanwhile, the martensite grows rapidly under pre-stress until the pre-stress unloading at 3 s. Then the speed of transformation returns to the state without pre-stress. Also, with the same pre-stress, unloading later causes more martensite during $t_2$ to $t_3(M_f)$.

The martensite transformation is finished at $t_u = 7s$, and the temperature is about 180 °C. The pre-stress plays a positive role until the transformation stops, so the fraction increases rapidly. Therefore, the growth of martensite will be the same unloading pre-stress after $t_3$, and the content curve is the same as unloading at 7 s ($t_3 < 7s$).

Therefore, pre-stress has a time-characteristic on microstructure transformation of the GH hardening layer.

In practical production, hardness is affected by the martensite content directly, and the retained austenite

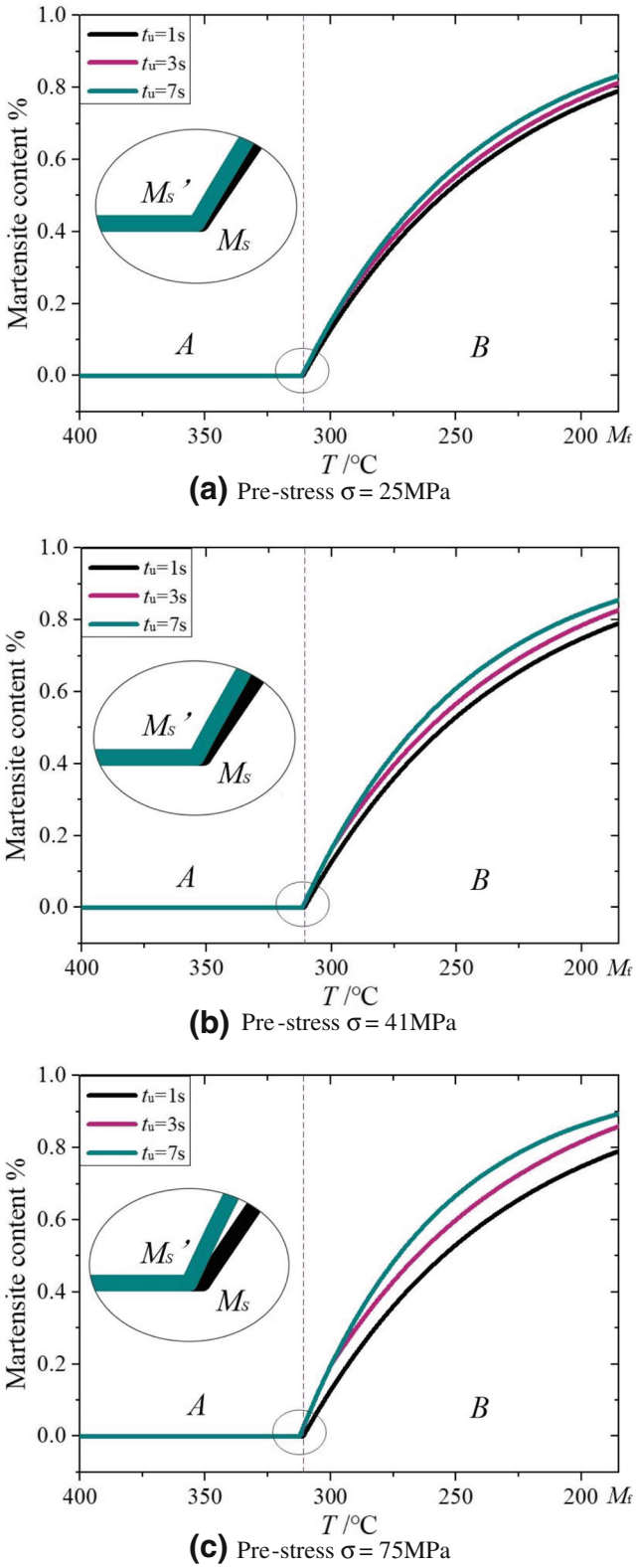


**Fig. 4** Martensite content under different unloading times and pre-stress: **a** pre-stress $\sigma = 25$ MPa, **b** pre-stress $\sigma = 41$ MPa, and **c** pre-stress $\sigma = 75$ MPa

can reduce the quenching deformation, improve the toughness of steel, or improve the dimensional stability of precision parts.

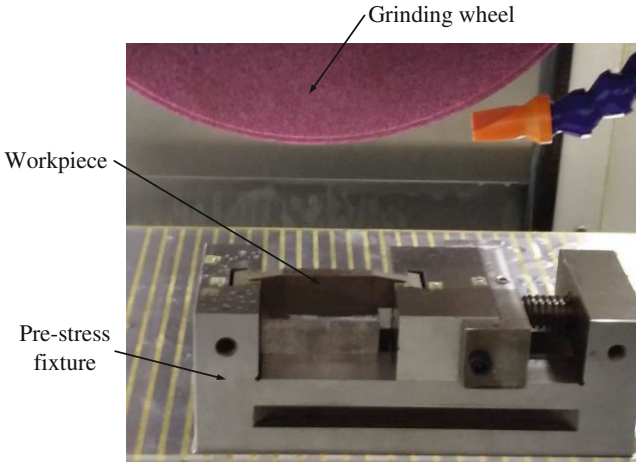


**Fig. 5** Experiment process of PSHG

## 4 Experiment

### 4.1 Experimental condition

The experiment is carried out on the surface grinder BLOHM ORBIT 36, and the corundum grinding wheel is chosen with the abrasive granularity F46. The wheel speed is 30 m/s and the wheel's diameter is 350 mm. Dry up-grinding is chosen to obtain the hardening layer by using the grinding heat. The size of the 1045 steel workpiece is 50 × 10 × 20 mm and it is fixed on the clamp, as seen in Fig. 5.

### 4.2 Technical parameters (Table 2)

Table 2 shows the technical parameters.

### 4.3 Analysis of martensite fraction in the microstructure

After grinding, the workpiece is cut along the cross-section and processed into a 10 × 10 × 15 mm cuboid. The mono-MMA is mixed with PMMA powder for a while and injected

**Table 2** Grinding parameters

| Workpiece no. | Pre-stress/ $\sigma$ (MPa) | Unloading time/$t_u$ (s) | Feed rate/$v_w$ (mm/min) | Grinding depth/$a_p$ (mm) |
|---|---|---|---|---|
| 1 | 25 | 1 | | |
| 2 | 25 | 3 | | |
| 3 | 25 | 7 | | |
| 4 | 41 | 1 | | |
| 5 | 41 | 3 | 200 | 0.15 |
| 6 | 41 | 7 | | |
| 7 | 75 | 1 | | |
| 8 | 75 | 3 | | |
| 9 | 75 | 7 | | |

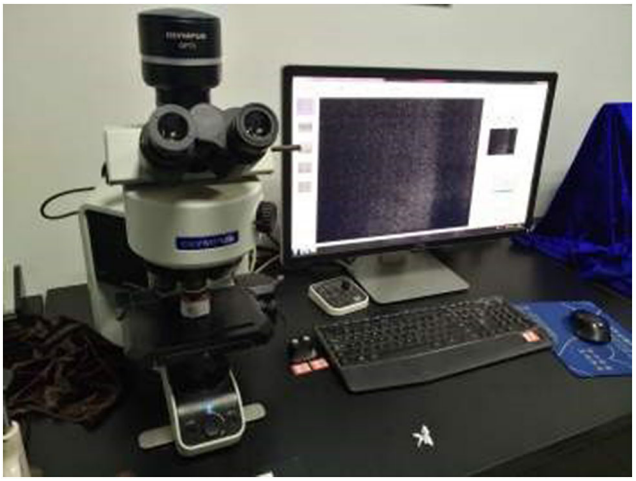

**Fig. 6** OLYMPUS metallographic microscope

**Table 3** The surface hardness under different pre-stress and unloading times

| Workpiece no. | Pre-stress /$\sigma$ (MPa) | Unloading time/$t$u (s) | Martensite content | Hardness (HV) |
|---|---|---|---|---|
| 1 | 25 | 1 | 79.3 | 744.6 |
| 2 | 25 | 3 | 81.8 | 748.5 |
| 3 | 25 | 7 | 83.2 | 761.1 |
| 4 | 41 | 1 | 74.3 | 773.2 |
| 5 | 41 | 3 | 76.2 | 797.3 |
| 6 | 41 | 7 | 77.3 | 826.3 |
| 7 | 75 | 1 | 74.4 | 749.4 |
| 8 | 75 | 3 | 76.6 | 752.3 |
| 9 | 75 | 7 | 77.4 | 767.2 |

into the mold containing the small cuboid block for vacuum cold mounting. Then, a cylinder sample of 30 mm in diameter and 15 mm in height is made and numbered.

The sample with different sizes of the sandpaper is ground, from coarse to fine. The direction of each grinding is vertical to that of the previous one, and the residual impurities and

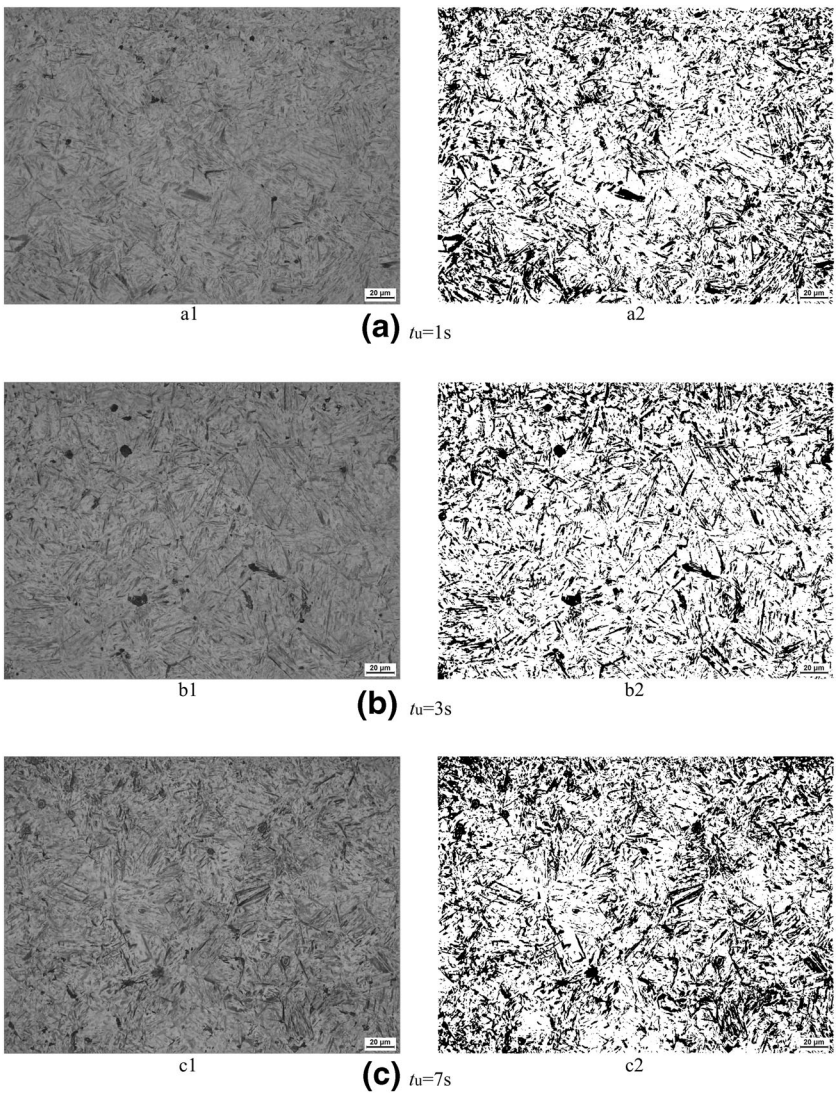


**Fig. 7** The martensite under different unloading times at $\sigma$ = 25 MPa

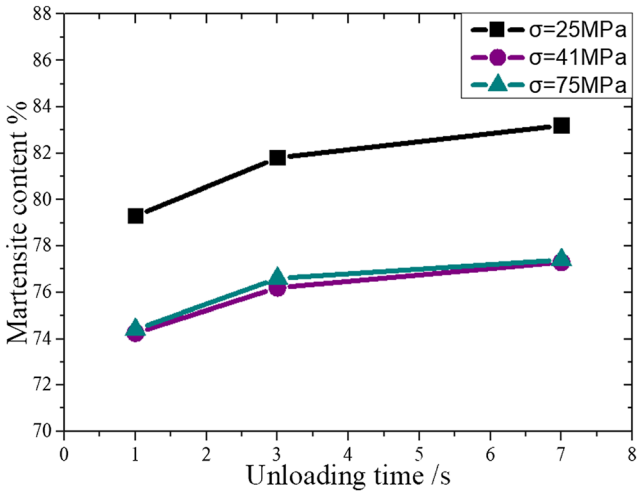


**Fig. 8** The martensite fraction under different unloading times

grinding marks on the surface are removed. Then, water grinding is carried out to make the surface smooth.

The sample is polished on the metallographic polishing machine to improve the smooth and bright, until its surface appears like a mirror.

The polished sample is cleaned and dried with a blower. Then, the sample is corroded with an alcohol solution containing 4% of nitric acid. Finally, the surface-treated is studied through the OLYMPUS metallography microscope, which is shown in Fig. 6.

The three pictures in Fig. 7 column 1 show the surface structure of the workpiece after PSHG with the pre-stress 25 MPa. It is difficult to distinguish the metallurgical structure. To observe the martensite, these pictures are processed, as shown in Fig. 7 column 2. The white region is martensite, and the black region includes residual austenite and undissolved carbide region. The

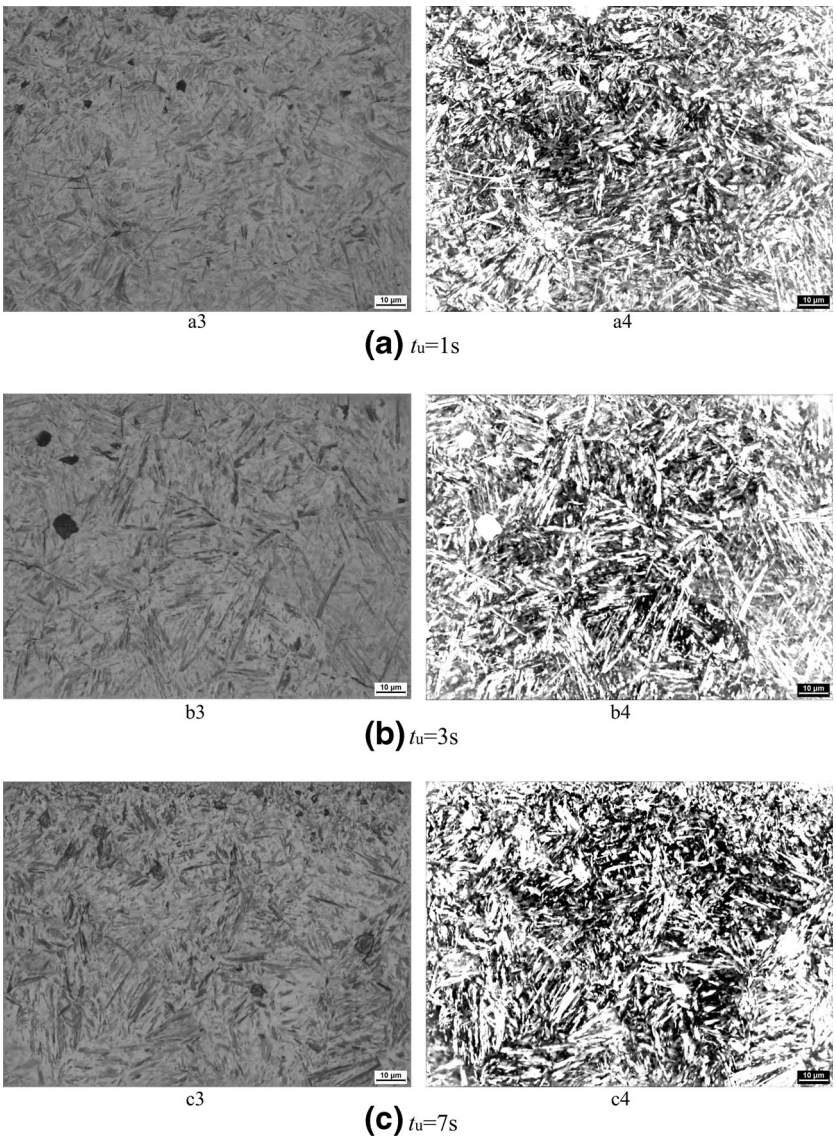


**Fig. 9** The flake martensite under different unloading times at $\sigma$ = 25 MPa: a $t$u = 1 s, **b** $t$u = 3 s, and **c** $t$u = 7 s

content of martensite in the hardening layer is obtained, too.

Figure 8 shows martensite fraction increases as the pre-stress unloading time goes on. The experimental results agree with the theory in section 3.

Besides, the hardness of the grinding surface under different pre-stress and unloading times is depicted in Table 3. Since martensite content affects hardness directly, it can be concluded the hardness of the workpiece's grinding layer improves with the increase of the pre-stress unloading time.

For medium carbon steels and some alloy steels, lath martensite forms at higher temperatures below $M_s$, and flake martensite forms at lower temperatures [33].

In order to observe flake martensite, the metallographic picture of 10 μm was obtained in Fig. 9 column 1. Another procession is taken as seen in column 2, because black is contributed to separate flake martensite.

Figure 10 shows the flake martensite pictures with pre-stress 41 MPa and 75 MPa. The flake martensite fraction is obtained in Fig. 11, as the pre-stress unloading time goes on the flake martensite fraction increases.

## 5 Conclusions

In this study, simulation, theoretical and experimental, is carried to study the effect of pre-stress time characteristic on GH.

Small pre-stress on the workpiece can raise the starting temperature of martensitic transformation during GH, and it can also promote the growth of martensite on the hardening layer.

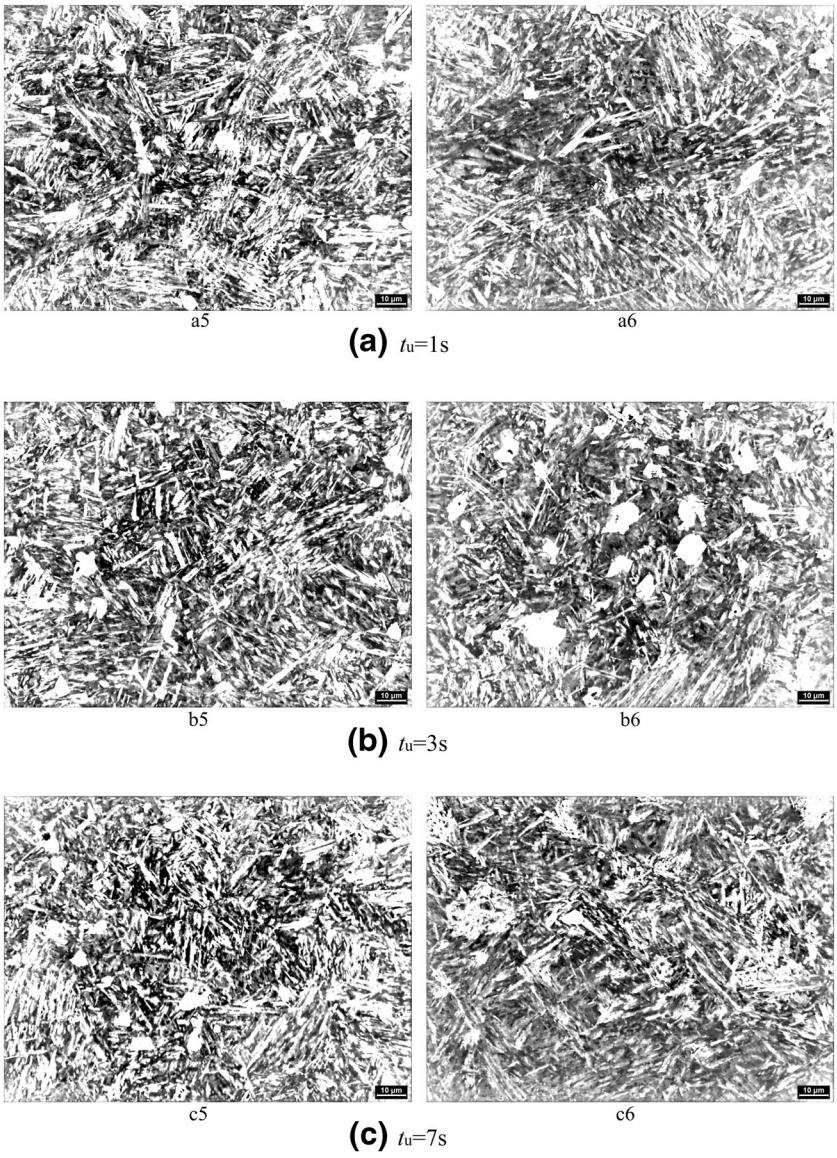


**Fig. 10** The flake martensite under different unloading times at $\sigma$ = 41 MPa(5) and 75 Mpa(6): a $t$u = 1 s, **b** $t$u = 3 s, and **c** $t$u = 7 s

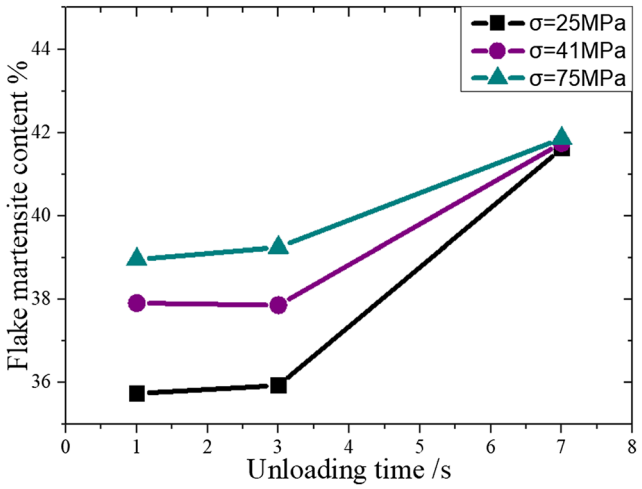


**Fig. 11** The flake martensite fraction under different unloading times

The trend of martensite content during cooling is almost the same unloading before $t_2(M_s)$. While unloading after $t_3(M_f)$, the trend is the same, too.

Unloading pre-stress during $t_2$ and $t_3$, the content of martensite in the hardening layer varies. The martensite content increases over the unloading time. Besides, an earlier unloading pre-stress can make the grinding surface more toughness, while a later unloading pre-stress can make the grinding surface more hardening.

For medium carbon steels and some alloy steels, lath martensite forms at a higher temperature below $M_s$, and flake martensite forms at a lower temperature. When the pre-stress releases at 1 s and 3 s, the pre-stress has little effect on the formation of flake martensite due to the high temperature. The pre-stress promotes more flake martensite when unloading at 7 s.

The pre-stress has time characteristic in grind hardening. The ideal microstructure can be obtained by effectively controlling the unloading time of pre-stress in a certain range.

**Funding information** This project is supported by the National Natural Science Foundation of China (Grant No. 51775101) and the Fundamental Research Funds for the Central Universities (N180306003).

## References

1. Yang M, Li C, Zhang Y, Jia D, Li R, Hou Y, Cao H, Wang J (2019) Predictive model for minimum chip thickness and size effect in single diamond grain grinding of zirconia ceramics under different lubricating conditions [J]. Ceram Int 45(12):14908–14920
2. Gao T, Zhang X, Li C, Zhang Y, Yang M, Jia D, Ji H, Zhao Y, Li R, Yao P, Zhu L (2020) Surface morphology evaluation of multi-angle 2D ultrasonic vibration integrated with nanofluid minimum quantity lubrication grinding [J]. J Manuf Process 51(1):44–61
3. Yang M, Li C, Zhang Y, Jia D, Li R, Hou Y, Cao H (2019) Effect of friction coefficient on chip thickness models in ductile-regime grinding of zirconia ceramics [J]. Int J Adv Manuf Technol 102: 2617–2632
4. Sun C, Niu Y, Liu Z, Xiu S (2017) Study on the surface topography considering grinding chatter based on dynamics and reliability [J]. Int J Adv Manuf Technol 92:3273–3286
5. Brinksmeier E, Brockhoff T (1996) Utilization of grinding heat as a new heat treatment process [J]. CIRP Ann Manuf Technol 45(1): 283–286
6. Zhang L, Ge P, Zhang J, Zhu Z, Luan Z (2007) Experimental and simulation studies on temperature field of 40Cr steel surface layer in grind-hardening [J]. Int J Abras Technol 1(2):187–197
7. Zarudi I, Zhang L (2002) Mechanical property improvement of quenchable steel by grinding [J]. J Mater Sci 37(18):3935–3943
8. Zhou N, Ru L, Pettersson R (2016) Surface integrity of 2304 duplex stainless steel after different grinding operations [J]. J Mater Processing Tech 229:294–304
9. Bruni C, Celeghini M, Geiger M, Gabrielli F (2007) A study of techniques in the evaluation of springback and residual stress in hydroforming [J]. Int J Adv Manuf Technol 33(9-10):929–939
10. Salonitis K, Kolios A (2015) Experimental and numerical study of grind-hardening-induced residual stresses on AISI 1045 Steel [J]. Int J Adv Manuf Technol 79(9-12):1443–1452
11. Wang J, Liu F, Feng Y, Gang Z (2011) Shot peening simulation based on SPH method [J]. Int J Adv Manuf Technol 56(5-8):571–578
12. Luh GC, Hwang RM (1998) Evaluating the effectiveness of vibratory stress relief by a modified hole-drilling method [J]. Int J Adv Manuf Technol 14(11):815–823
13. Xiu S, Shi X (2015) Transformation mechanism of microstructure and residual stress within hardening layer in PSHG [J]. Journal of Advanced Mechanical Design Systems & Manufacturing 9(3):1–13
14. Deng Y, Xiu S, Shi X, Sun C, Wang Y (2016) Study on the effect mechanisms of pre-stress on residual stress and surface roughness in PSHG [J]. Int J Adv Manuf Technol 88:3243–3256
15. SHI X, XIU S, ZHANG X, WANG Y (2017) A study of PSHG and its characteristic mechanism of residual stress within a hardened layer [J]. Int J Adv Manuf Technol 88:863–877
16. Kim NK, Guo C, Malkon S (1997) Heat flux distribution and energy partition in creep-feed grinding [J]. CIRP Ann Manuf Technol 46(1):227–232
17. Zhou L, Huang ST, Zhang CY (2013) Numerical and experimental studies on the temperature field in precision grinding of SiCp/Al composites [J]. Int J Adv Manuf Technol 67(5-8):1007–1014
18. Yao C, Wang T, Xiao W, Huang X, Ren J (2014) Experimental study on grinding force and grinding temperature of Aermet 100 steel in surface grinding [J]. J Mater Process Technol 214(11): 2191–2199
19. Rowe WB, Jin T (2001) Temperatures in high efficiency deep grinding (HEDG) [J]. CIRP Ann Manuf Technol 50(1):205–208
20. Ramanath S, Ramaraj T, Shaw M (1987) What grinding swarf reveals [J]. CIRP Ann Manuf Technol 36(1):245–247
21. Ramanath S, Shaw M (1988) Abrasive grain temperature at the beginning of a cut in fine grinding [J]. J Eng Ind 110(1):15–18
22. Niu Y, Sun C, Pang G, XIu S. Study on the effect of pre-stress unloading time on surface integrity in PSHG process [J]. 2018,
23. Reynolds J, Bever M (1952) On the reversal of the strain-induced martensitic transformation in the copper-zinc system [J]. JOM 4(10):1065–1066
24. McReynolds A (1949) Effects of stress and deformation on the martensite transformation [J]. J Appl Phys 20(10):896–907
25. Hsu T, Hongbing C, Shoufu L On thermodynamic calculation of MS and on driving force for martensitic transformations in Fe-C [J]. J Mater Sci 18(11):3206–3212
26. Sun C, Liu Z, Lan D, Duan J, Xiu S Study on the influence of the grinding chatter on the workpiece's microstructure transformation [J]. International Journal of Advanced Manufacturing Technology 96:3861–3879

27. Tamura I (2015) Deformation-induced martensitic transformation and transformation-induced plasticity in steels [J]. Metal Sci 16(5): 245–253
28. Ledbetter H, Dunn ML Habit planes, inclusion theory, and twins [J]. Mater Sci Eng A 273-275(none):222–225
29. Patel JR, Cohen M Criterion for the action of applied stress in the martensitic transformation [J]. 1(5):531–538
30. Koistinen D, Marburger R (1959) A general equation prescribing the extent of the austenite-martensite transformation in pure iron-carbon alloys and plain carbon steels [J]. Acta Metall 7(1):59–60
31. Sherman D, Yang B, Catalina A, Hattiangadi A, Zhao P, Chuzhoy L, Johnson M (2007) Modeling of microstructure evolution of a thermal transformation of lath martensite [C]. Mater Sci Forum 539-543:4795–4800
32. Zuchang Z Martensitic Transformation (5) [J]. Heat Treatment Technol Equip 03:71–74
33. Krauss G, Marder A (1971) The morphology of martensite in iron-carbon alloys [J]. Metall Trans A 2(9):2343–2357